DELFT UNIVERSITY OF TECHNOLOGY

REPORT 13-05

ISOGEOMETRIC SHAPE OPTIMIZATION OF MAGNETIC DENSITY SEPARATORS

NGUYEN DANG MANH, ANTON EVGRAFOV, JENS GRAVESEN AND DOMENICO LAHAYE

ISSN 1389-6520

Reports of the Department of Applied Mathematical Analysis

Delft 2013

Isogeometric Shape Optimization of Magnetic Density Separators

Nguyen Dang Manh[a], Anton Evgrafov[b], Jens Gravesen[b], Domenico Lahaye[c]

[a] *Department of Applied Mathematics, SINTEF Information and Communication Technology, Forskningsveien 1, N–0373 Oslo, Norway*
[b] *Department of Applied Mathematics and Computer Science, Technical University of Denmark, Matematiktorvet, Building 303B, DK-2800 Kgs. Lyngby, Denmark*
[c] *Delft Institute for Applied Mathematics, Delft University of Technology, Mekelweg 4, 2628 CD Delft, The Netherlands*

Abstract

Purpose: The waste recycling industry increasingly relies on magnetic density separators. These devices generate an upward magnetic force in ferro-fluids allowing to separate the immersed particles according to their mass density. Recently a new separator design that significantly reduces the required amount of permanent magnet material has been proposed. The purpose of this paper is to alleviate the undesired end-effects in this design by altering the shape of the ferromagnetic covers of the individual poles.

Design/methodology/approach: We represent the shape of the ferromagnetic pole covers with B-splines and define a cost functional that measures the non-uniformity of the magnetic field in an area above the poles. We apply an isogeometric shape optimization procedure, which allows us to accurately represent, analyse and optimize the geometry using only a few design variables. The design problem is regularized by imposing constraints that enforce the convexity of the pole cover shapes and is solved by a non-linear optimization procedure. We validate the implementation of our algorithm using a simplified variant of our design problem with a known analytical solution. The algorithm is subsequently applied to the problem posed.

Research limitations/implications: The shape optimization attains its target and yields pole cover shapes that give raise to a magnetic field that is uniform over a larger domain. This increased uniformity is obtained at the cost of a pole cover shape that differs per pole. This limitation has negligable impact on the manufacturing of the separator. The new pole cover shapes therefore lead to improved performance of the density separation.

Originality/value: This paper treats the shapes optimization of magnetic density separators systematically and presents new shapes for the ferromagnetic poles covers. Due to the larger uniformity the generated field, these shapes should enable larger amounts of waste to be processed than the previous design.

Keywords: Magnetic density separation, shape optimization, isogeometric analysis

1. Introduction

Magnetic density separators are increasingly being used by the waste recycling industry. The development and usage of these devices is extensively described in e.g. the monograph [1]. The separators considered here exert an upward magnetic force on waste particles immersed in a container with ferrofluid. As the magnitude of the resultant of the hydrostatic and magnetic buoyancy force is proportional to the mass density of the waste particles, these particles will float at mass density specific heights. If this height is constant across lateral directions in the container, particles of the same mass density can easily be removed from the container.

The requirements imposed on the magnetic field led to the development of permanent magnet arrays specifically for magnetic density separators [2, 3]. Very recently, a design that significantly reduces the amount of costly permanent magnet material was proposed [4]. Given its importance in this paper, this design is shown in Figure 1.

Figure 1(a) shows a front view of the Hallbach-type magnet array considered. Only the part to the configuration to the right of the vertical symmetry axis is depicted. The configuration consists of three permanent magnet poles interleaved by ferromagnetic poles mounted on an iron back plate. All magnets are magnetized upward as indicated by the arrows in the figure. Both the magnet and iron poles are covered by iron caps such that the magnet field above the array is suitably shaped. Assuming that the structure is continued periodically, an analytical expression for the pole cover shape has been derived in [4]. This expression will be reviewed in Subsection 5.1 of this paper. In case that the array is truncated to finite length however, end effects in the magnetic field do appear as shown in Figure 1(b). This figure shows the magnitude of the simulated magnetic field as a function of the lateral coordinate x at three values of the height coordinate y. For the simulation we employ two-dimensional finite element simulations. The occurrence of the end effects shown perturbs the uniformly of the magnetic field above the array and severely limits the deployment of the magnet array for density separation.

Figure 5(a)-(b) in Subsection 5.2 shows that the end effects can already be significantly reduced by permuting the role of magnet and iron poles. To goal of this paper is to apply shape optimization of the pole coverings in the configurations shown in Figure 5(a)-(b) in order to further reduce the end-effects. Various approaches to shape optimization of stationary magnetic fields has been proposed by various authors. Without the intention of giving an overview, we here list some references [5–9]. In this paper we propose to use iso-geometric analysis.

Isogeometric analysis is a modern numerical method for solving partial differential equations [10, 11]. Its name stems from the fact that the same class of functions is used to parametrize the geometry and to solve the differential equation. The computational domain is subdivided into a number of patches such that each patch is the image of the reference element under a parametrization. This parametrization is defined as a linear combination of the tensor products of B-splines. The use of splines in the geometry modeling allows to represent complex computational domains with a limited number of design variables. On each patch the basis functions are as the composition of the pull-back operator and the tensor product of spline basis function on the reference elements.

Email addresses: manhiga@gmail.com (Nguyen Dang Manh), aaev@dtu.dk (Anton Evgrafov), jgra@dtu.dk (Jens Gravesen), d.j.p.lahaye@tudelft.nl (Domenico Lahaye)

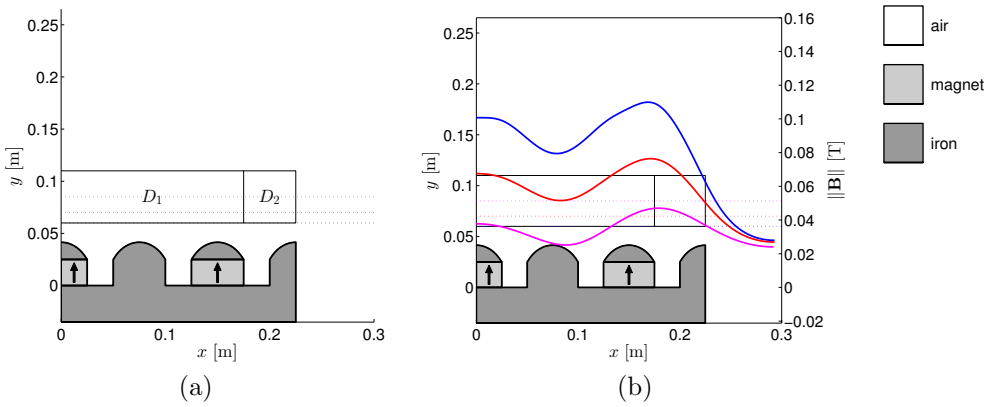

Figure 1: Front view of the magnet array proposed in [4] with the objective domains D_1 and D_2 (left). Computed magnetic flux at a height equal to 6, 7 and 8.5 cm above the back plate (right).

This choice allows to continuously vary the basis functions with the underlying shape and avoids the introduction of numerical noise associated with mesh updating procedures associated with traditional FEM procedures. The advantages of isogeometric analysis for shape optimization are described in e.g. [12–14].

In this paper we apply iso-geometric shape optimization to the magnetic density separators shown in Figure 5(a)-(b). Our goal is to shape the covers of the individual poles in such a way to minimize the non-uniformity of the field above the poles. We introduce a functional that measures the field non-uniformity and minimize this functional over two objective domains to investigate the influence of the end-effects. Our algorithm produces new shapes that significantly improve the field uniformity and that therefore renders the device much more useful in industrial applications.

This paper is structured as follows: in Section 2 we describe the shape optimization problem we set out to solve. In Section 3 we briefly review the iso-geometric analysis and shape optimization technique that we intend to employ. In Section 4 we give more details on the shape representation using B-splines as it is an essential ingredient in the approach that we adopt. In Section 5 the methodology we advocate is tested on a design problem with a known analytical solution and on two versions of the shape optimization problem of the magnetic density separator. In Section 6 finally conclusions are drawn.

2. Formulation of the Shape Optimization Problem

In this section we formulate the shape optimization problem of the magnet array shown in Figure 5(a)-(b) by giving details of the magnetic field equation, the cost functional, the design variables and the regularization technique.

The objective of the shape optimization is to find shapes of the covers of the magnet and ferromagnetic poles that yield a magnetic field distribution that is better suited for the density separation on waste particles immersed in the ferro-fluid in the container placed in the magnetic field. Such particles experiences the downward gravitational pull,

the upward hydrostatic buoyancy force and the upward magnetic force from the ferro-fluid. If the latter is made independent of the lateral (x-) coordinate, the resultant force is laterally invariant as well, and waste particles with the same mass density will float at an laterally invariant height. This facilitates the removal of the different particles from the fluid and renders the device attractive from an industrial point of view.

A ferro-fluid with mass density ρ_f and saturation magnetization M_f will react to being placed in a spatially varying magnetic field $\mathbf{B}(x, y)$ by a change in its density to its so-called apparent density ρ_{app}. The latter is proportional to the gradient of the magnitude magnetic field in the y-direction $\partial\|\mathbf{B}\|/\partial y$. More precisely, we have that [1, 15]

$$\rho_{app} = \rho_f + \frac{M_f}{g}\frac{\partial\|\mathbf{B}\|}{\partial y}, \tag{1}$$

where g is the gravitational constant. The upward force by the ferro-fluid is proportional its apparent density ρ_{app}. The condition of the lateral invariance of the force by the ferro-fluid can therefore be expressed as

$$\frac{\partial^2\|\mathbf{B}\|}{\partial x\,\partial y} = 0\,. \tag{2}$$

Our objective is therefore to enforce this condition, at least approximately, over a rectangular region Ω_0 located above the magnet array.

We will compute the magnetic field generated by the magnet array using a vector potential formulation [16]. In two-dimensional perpendicular plane configurations and in the presence of vertically (y-) magnetized permanent magnets with remanent flux density $\mathbf{B}_r = (0, B_r, 0)$, the double curl equation for the vector potential $\mathbf{A} = (0, 0, A_z(x, y))$ reduces to

$$-\frac{\partial}{\partial x}\left(\frac{1}{\mu}\frac{\partial A_z}{\partial x}\right) - \frac{\partial}{\partial y}\left(\frac{1}{\mu}\frac{\partial A_z}{\partial y}\right) = \frac{1}{\mu}\frac{\partial B_r}{\partial x}\,, \tag{3}$$

where the relative magnetic permeability μ_r is set to 1000 and to 1 in the iron and permanent magnet domain, respectively. The magnets in our simulations have a strength of $B_r = 1.235\,\mathrm{T}$. The field equation is supplied with an insulation boundary condition.

In order to avoid the introduction of third order derivatives of A_z in the objective function, we replace Condition (2) by the minimization of the dispersion of $\partial\|\mathbf{B}\|/\partial y$ in x-direction, i.e., we aim at reducing the difference between $\partial\|\mathbf{B}\|/\partial y$ and its average value along horizontal lines in Ω_0. This motivates to define, for a given value of y, the dispersion $\mathbb{D}(y)$ as

$$\begin{aligned}\mathbb{D}(y) &= \int_{x_1}^{x_2}\left(\frac{\partial\|\mathbf{B}\|}{\partial y}\,\mathrm{d}x - \frac{1}{x_2 - x_1}\int_{x_1}^{x_2}\frac{\partial\|\mathbf{B}\|}{\partial y}\,\mathrm{d}x\right)^2\mathrm{d}x \\ &= \int_{x_1}^{x_2}\left(\frac{\partial\|\mathbf{B}\|}{\partial y}\right)^2\mathrm{d}x - \frac{1}{x_2 - x_1}\left(\int_{x_1}^{x_2}\frac{\partial\|\mathbf{B}\|}{\partial y}\,\mathrm{d}x\right)^2 .\end{aligned} \tag{4}$$

In this study we will minimize the average dispersion over objective domains of the form

$\Omega_0 = [x_1, x_2] \times [y_1, y_2]$, resulting in the following form of the cost functional

$$\begin{aligned} I_0[A_z; \Omega_0] &= \int_{y_1}^{y_2} \mathbb{D}(y)\, dy \\ &= \int_{y_1}^{y_2} \left[\int_{x_1}^{x_2} \left(\frac{\partial \|\mathbf{B}\|}{\partial y} \right)^2 \mathrm{d}x - \frac{1}{x_2 - x_1} \left(\int_{x_1}^{x_2} \frac{\partial \|\mathbf{B}\|}{\partial y}\, \mathrm{d}x \right)^2 \right] \mathrm{d}y\,. \end{aligned} \tag{5}$$

In this functional only derivatives of A_z up to order two appear. Numerical experiments in Section 5, in which we will seek to minimize $\log_{10}[I_0/\mathrm{area}(\Omega_0)]$, will give evidence that the cost functional (5) is indeed appropriately chosen.

We will conduct numerical studies on the configuration shown in Figure 5(a)-(b) for two choices for the objective domain Ω_0. We define the subdomains D_1 and D_2 shown in Figure 1 by

$$\begin{aligned} D_1 &= [0, 0.175] \times [0.06, 0.11] \quad [\mathrm{m} \times \mathrm{m}] \\ D_2 &= [0.175, 0.225] \times [0.06, 0.11] \quad [\mathrm{m} \times \mathrm{m}]\,, \end{aligned} \tag{6}$$

respectively. We set Ω_0 equal to the domain $D_1 \cup D_2$ in the first study. In the second we restrict the objective domain to the interior by setting $\Omega_0 = D_1$.

We will represent the shape of the ferromagnetic pole covers using B-splines and use the y-coordinates of the control points shown in Figure 2 as design variables. Convexity constraints are imposed to regularize the design problem by avoiding shapes with strong oscillations or sharp corners as shown in [13].

3. Isogeometric shape optimization

In this section we briefly describe the iso-geometric analysis (IGA) method for solving the magnetic field equation (3) and for the shape optimization of the magnetic density separator shown in Figure 5(a)-(b). We refer to [10–14] for more details.

3.1. Isogeometric Analysis

The IGA method employs the same basis functions to represent both the geometry and the discrete solution of the field equation. In this way the method is similar to the iso-parametric finite element method. The IGA method however uses a more global parametrization of the geometry than classical finite element methods by decomposing the computation domain into a set of patches $\Omega = \cup_\alpha \Omega_\alpha$. Such a decomposition for the magnetic density separator shown in Figure 5(a)-(b) into a set of 30 patches is shown in Figure 2. In this figure, the ferromagnetic poles with patch number 2 and 17 are parametrized as a single patch while the magnetic poles with patch number 10, 11, 24 and 25 are parametrized using two patches to allow the ferromagnetic caps to cover the magnets. Patches number 3, 6, 12, 15, 18, 21 and 26 and the remaining patches correspond to the ferromagnetic back plate and the air region, respectively. The top boundary of the ferromagnetic and magnetic poles will be allowed to change during the shape optimization process. The global handling of the geometry by patches will facilitate adopting the discretization to changes in the geometry in the next section.

Given the well-documented versatility of splines to represent complex shapes, the IGA method use these functions as basis functions. In this work we adopt B-splines.

Let u and v denotes the coordinates in the parameter space $[0,1]^2$. Let h denote the mesh width of an equidistant mesh on $[0,1]$. We will parametrize the patch Ω_α using B-splines of order p and q with knot vectors Ξ_u^α and Ξ_v^α denoted by $M_i^{\alpha,p}(u)$ and $N_j^{\alpha,q}(v)$, respectively. Given the knot vector

$$\Xi_u^\alpha = \{ \underbrace{0,\ldots,0}_{p+1 \text{ times}}, h, 2\,h, \ldots, 1-2\,h, 1-h, \underbrace{1,\ldots,1}_{p+1 \text{ times}} \}, \tag{7}$$

the set of splines $M_i^{\alpha,p}(u)$ is constructed as a linear combination of products of lower order splines. A similar argument holds for the construction $N_j^{\alpha,q}(v)$ given Ξ_v^α. We will expand the discrete solution on a patch using the same B-splines. We will denote the tensor product of splines by $R_{ij}^{\alpha,pq}(u,v) = M_i^{\alpha,p}(u) N_j^{\alpha,q}(v)$.

Each patch Ω_α is parametrized by a linear combination of tensor products of the geometry splines, i.e., $\mathbf{F}_\alpha : [0,1]^2 \to \Omega_\alpha$ where

$$\mathbf{F}_\alpha(u,v) = \big(x_\alpha(u,v), y_\alpha(u,v)\big) = \sum_{i=1}^{m}\sum_{j=1}^{n} \mathbf{d}_{ij}\, R_{ij}^{\alpha,pq}(u,v)\,, \tag{8}$$

where $\mathbf{d}_{ij}$ are the *control* points. To highlight the dependence of $\mathbf{F}_\alpha(u,v)$ on the control points, we will use the notation $\mathbf{F}_\alpha(u,v;\mathbf{d})$. We use spline degree $p = 3 = q$ on all patches. We will distinguish between patches whose shape is fixed and variable during the design process. On the latter patches, we will treat the *boundary* and *interior* control points separately. To control the shape of the boundary of a design-variable patch, we perform a uniform $h \to H$ coarsening of the corresponding knot vector (7) to obtain

$$\widehat{\Xi}_u^\alpha = \{ \underbrace{0,\ldots,0}_{p+1 \text{ times}}, H, 2\,H, \ldots, 1-2\,H, 1-H, \underbrace{1,\ldots,1}_{p+1 \text{ times}} \}, \tag{9}$$

and designate the x and y-coordinates of the corresponding control points as design variables. In this construction knot vectors required for the boundary parametrization of $\mathbf{F}_\alpha$ are obtained by inserting points uniformly in the knot vector used to describe shape variations. Consequently, the boundary control points are linear combinations of the design control points. This allows to update of the parametrization of an entire patch to shape variations of its boundary and is the distinct feature of the shape optimization using IGA method. This procedure will be outlined in more details in the next section. Figure 2 illustrates this division in control points for the patches corresponding to the magnet ($\alpha = 10, 11, 24, 25$) and ferromagnetic ($\alpha = 2, 17$) poles. The y-coordinate of the variable boundary control points of patch number 2, 7, 10 and 24 add up to a total of 22 design variables.

On each patch the basis functions are defined by composing the inverse of the parametrization $\mathbf{F}_\alpha$ (also referred to as the pull-back operator) with the tensor of two analysis splines to obtain $R_{ij}^{\alpha,pq}(u,v) \circ \mathbf{F}_\alpha^{-1}(x,y)$. The discrete approximation $u(x,y)$ to the magnetic vector potential over Ω_α can be expanded in this basis as

$$u(x,y) = \sum_{i}^{m}\sum_{j}^{n} h_{ij}^{\alpha} R_{ij}^{\alpha,pq}(u,v) \circ \mathbf{F}_\alpha^{-1}\,. \tag{10}$$

To determine the expansion coefficients h_{ij}^{α}, we proceed as in any classical finite element method and cast the magnetic field equation (3) in a Galerkin variational formulation. The resulting integrals over Ω_α can be transformed into integrals over $[0,1]^2$

$$\iint\limits_{\Omega_\alpha} f(x,y)dx\,dy = \int_0^1 \int_0^1 f\big(x_\alpha(u,v), y_\alpha(u,v)\big)\,\det(\mathbf{J}_\alpha)\,du\,dv\,, \tag{11}$$

where $\mathbf{J}_\alpha = \partial \mathbf{F}_\alpha / \partial(u,v)$ denotes the Jacobian of $\mathbf{F}_\alpha$, and evaluated via Gaussian quadrature. The weak form on Ω_α then leads to the system of algebraic equations $\mathbf{K}^\alpha\,\mathbf{h}^\alpha = \mathbf{f}^\alpha$, where $\mathbf{h}^\alpha$ contains the coefficients h_{ij}^α. The entries of $\mathbf{K}^\alpha$ are of the form

$$\mathbf{K}^\alpha_{k,\ell} = \frac{1}{\mu}\int_0^1 \int_0^1 \left(\nabla R_k\,\mathbf{J}_\alpha^{-1}\right)^T \left(\nabla R_\ell\,\mathbf{J}_\alpha^{-1}\right) \det \mathbf{J}_\alpha\,\mathrm{d}u\,\mathrm{d}v\,, \tag{12}$$

where the indices k and ℓ correspond to a lexicografic ordering of the unknowns. Given that patches number 11 and 25 are formed by vertically magnetized magnets of size h_m and strength M_0, the entries of $\mathbf{f}^\alpha$ are of the form

$$\mathbf{f}^\alpha_\ell = \begin{cases} M_0\,h_m \int_0^1 (R_\ell(1,v) - R_\ell(0,v))\,\mathrm{d}v & \text{if } \alpha = 11 \text{ or } \alpha = 25\,, \\ 0 & \text{otherwise}\,. \end{cases} \tag{13}$$

Imposing the continuity of both the domain parametrization and the field solution along the patch boundaries results in linear dependencies of a number of control points and expansion coefficients corresponding to neighbouring patches. These can easily be eliminated from the final system as detailed in [13]. Collecting the contributions from every patch we obtain a system of linear equations

$$\mathbf{K}\,\mathbf{h} = \mathbf{f}\,, \tag{14}$$

where $\mathbf{h}$ contains the expansion coefficients of the solutions on all patches.

3.2. Shape sensitivity analysis

To be able to solve the shape optimization problem by a gradient-based optimization algorithm, the first order sensitivity of the cost functional (5) constrained by the magnetic field equation (3) needs to be computed. To this end, we proceed in a standard way (see e.g. [14]). The derivative of the discrete magnetic field solution with respect to the boundary control points $\mathbf{d}_{ij}$ for instance can be found by solving the auxiliary system of linear equations

$$\mathbf{K}\,\frac{\partial \mathbf{h}}{\partial \mathbf{d}_{ij}} = \frac{\partial \mathbf{f}}{\partial \mathbf{d}_{ij}} - \frac{\partial \mathbf{K}}{\partial \mathbf{d}_{ij}}\,\mathbf{h}, \tag{15}$$

obtained by differentiating the system (14). Here we have that $\partial \mathbf{f}/\partial \mathbf{d}_{ij} = \mathbf{0}$. The derivative $\partial \mathbf{K}/\partial \mathbf{d}_{ij}$ can be computed by integration over the reference domain. The optimization problem is solved using SQP implemented in MATLAB's `fmincon` function using as initial guess the shapes shown in Figure 2.

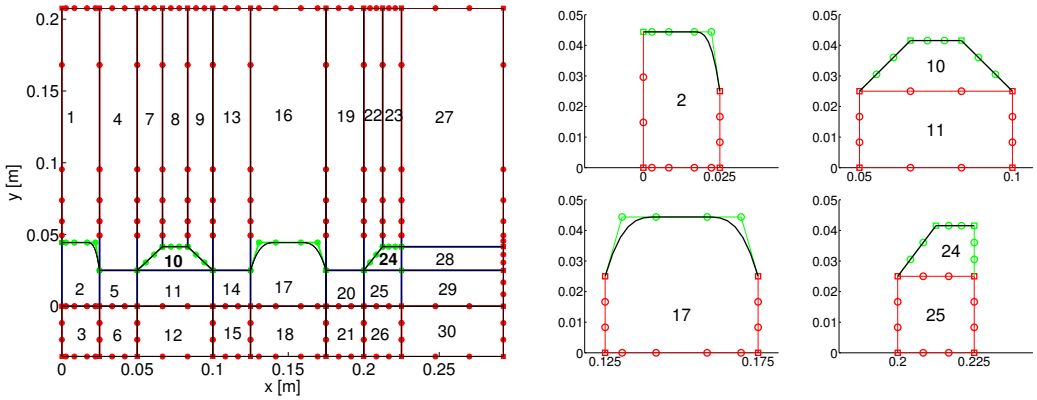

Figure 2: Decomposition of the computational domain Ω into a set of 30 patches Ω_α (left). Detailed view on the four poles with the boundary control points indicated. (right).

3.3. Shape regularization by imposing convexity

We regularize the shape optimization algorithm by imposing the convexity of the shape of the ferromagnetic pole covers. This results in a set of simple linear equality and inequality constrains on the control points, which are added to the shape optimization problem.

4. Domain Parametrization using B-Splines

In this section we discuss the techniques that we employ to construct a parametrization $\mathbf{F}_\alpha$ defined in (8) of a patch Ω_α that is both invertible and of sufficiently high quality. Given the parametrization of the boundary of Ω_α that typically results from a shape updating step in the optimization process, our goal is to compute the control points $\mathbf{d}$ corresponding to the interior control points that satisfy both requirements on $\mathbf{F}_\alpha$. The difficulty of this task increases with the geometrical complexity of Ω_α. Given that the procedures to find $\mathbf{d}$ have to be applied within each step of an outer optimization algorithm, it is of paramount importance to keep their computational complexity limited.

To ensure regularity of $\mathbf{F}_\alpha(u,v)$ we require that given some $\epsilon > 0$, the Jacobian $\mathbf{J}_\alpha(u,v)$ satisfies $\det(\mathbf{J}_\alpha(u,v)) \geq \epsilon$ for all $(u,v) \in (0,1)^2$. We denote by $\det[\mathbf{d}_{ij}, \mathbf{d}_{k\ell}]$ the determinant of the 2×2 matrix formed by the x and y-coordinates of $\mathbf{d}_{ij}$ and $\mathbf{d}_{k\ell}$. Differentiating (8), we obtain

$$\begin{aligned} \det(\mathbf{J}_\alpha(u,v)) &= \sum_{i,j=1}^{m} \sum_{k,\ell=1}^{n} \det[\mathbf{d}_{ij}, \mathbf{d}_{k\ell}] \, \frac{\mathrm{d}M_i^{\alpha,p}(u)}{\mathrm{d}u} \, N_j^{\alpha,q}(v) M_k^{\alpha,p}(u) \, \frac{\mathrm{d}N_\ell^{\alpha,q}(v)}{\mathrm{d}v} \\ &= \sum_{i=1}^{2m-1} \sum_{j=1}^{2n-1} c_{ij} \, M_i^{\alpha,2p-1}(u) \, N_j^{\alpha,2q-1}(v) \,, \end{aligned} \tag{16}$$

where $M_i^{\alpha,2p-1}(u)$ and $N_j^{\alpha,2q-1}(v)$ are B-splines of order $2p-1$ and $2q-1$ over the patch Ω_α, respectively, and to where to each of the coefficients c_{ij} corresponds a quadratic form determined by the square symmetric matrix Q_{ij} such that [17]

$$c_{ij} = \mathbf{d}^T Q_{ij} \mathbf{d} \,. \tag{17}$$

Given that the B-splines are positive, the regularity of $\mathbf{F}_\alpha(u,v)$ can be ensured by imposing that each of the coefficients c_{ij} in (16) is positive.

To ensure that a parametrization $\mathbf{F}_\alpha$ is of high quality we require the matrix $\mathbf{g}_\alpha = \mathbf{J}_\alpha^T \mathbf{J}_\alpha$ to be well approximated by the identity (see e.g. Corollary 6.4.3 in [18]). To this end we introduce the *Winslow functional* $W[\mathbf{F}_\alpha(\mathbf{d})]$ [19] defined by

$$W[\mathbf{F}_\alpha(\mathbf{d})] = \iint_{[0,1]^2} \mathcal{W}[\mathbf{F}_\alpha(u,v;\mathbf{d})] \, du \, dv \,, \tag{18}$$

where for over $(u,v) \in (0,1)^2$ the integrand $\mathcal{W}[\mathbf{F}_\alpha(u,v;\mathbf{d})]$ is given by

$$\mathcal{W}[\mathbf{F}_\alpha(u,v;\mathbf{d})] = \frac{\operatorname{trace}(\mathbf{g}_\alpha)}{\sqrt{\det(\mathbf{g}_\alpha)}} = \frac{\lambda_1 + \lambda_2}{\sqrt{\lambda_1 \lambda_2}} = \frac{\|\partial \mathbf{F}_\alpha / \partial u\|_2 + \|\partial \mathbf{F}_\alpha / \partial v\|_2}{\det(\mathbf{J}_\alpha)} \,, \tag{19}$$

and where λ_1 and λ_2 denote the eigenvalues of $\mathbf{g}_\alpha$. A high quality of $\mathbf{F}_\alpha$ then corresponds to as low value of $W[\mathbf{F}_\alpha(\mathbf{d})]$ as possible. Minimizing $W[\mathbf{F}_\alpha(\mathbf{d})]$ over the feasible set of control points $\mathbf{d}$ that yield positive coefficients c_{ij} is however too computationally demanding to be carried out at every step of the outer optimization algorithm. We therefore resort to a two-stage heuristic in which in the first stage a reference parametrization is found by solving the afore mentioned constrained optimization problem. In the second stage the parametrization is updated to changes in the geometry at small computational cost. In case that the update fails to result in positive coefficients c_{ij}, the reference parametrization is updated in a process similar to remeshing in the classical finite element methods. In the remainder of this section, we give more details of both of these stages.

4.1. Constructing a Reference Parametrization

In the first stage we construct a reference parametrization denoted by $\mathbf{d}_0$ by minimizing the Winslow functional (18) over the design space of spline control points $\mathbf{d}$ subject to the constraint that the coefficients c_{ij} defined by (17) remain positive. This optimization problem is solved to local optimality using a non-linear optimization method.

4.2. Updating the Parametrization to the Current Geometry

In the second stage we update the reference parametrization $\mathbf{d}_0$ to the current shape of the patch Ω_α by minimizing the second order Taylor polynomial of the Winslow functional (18) around the point $\mathbf{d}_0$. This polynomial can be written as

$$W[\mathbf{F}_\alpha(\mathbf{d})] \approx W[\mathbf{F}_\alpha(\mathbf{d}_0)] + G(\mathbf{d}_0)(\mathbf{d}_0 - \mathbf{d}) + {}^1\!/_2 (\mathbf{d}_0 - \mathbf{d})^T H(\mathbf{d}_0)(\mathbf{d}_0 - \mathbf{d}) \,, \tag{20}$$

where $G(\mathbf{d}_0)$ and $H(\mathbf{d}_0)$ denote the gradient and Hessian of $W[\mathbf{F}_\alpha]$ with respect to the control points $\mathbf{d}$ evaluated in the point $\mathbf{d}_0$, respectively. Minimizing this polynomial is then equivalent to solving the *linear* system of equations

$$H(\mathbf{d}_0)(\mathbf{d}_0 - \mathbf{d}) = -G(\mathbf{d}_0) \,, \tag{21}$$

resulting in an inexpensive updating formula.

5. Numerical experiments

This section consists of two subsections. In Subsection 5.1 we validate our isogeometric shape optimization algorithm on a synthetic problem for which an analytical expression for the optimal shape is known. In Subsection 5.2 we solve the design problem of the magnet array shown in Figure 5(a)-(b).

5.1. Synthetic Problem with Analytical Expression for the Optimal Shape

In this subsection we show that in the absence of end effects the analytical expression for the optimal shape of the pole cover given in [4] can be derived. We subsequently employ this expression to validate the implementation of our shape optimization algorithm by verifying that the difference between the numerically and analytically determined shapes converges to zero at a rate that increases with the polynomial order of the spline approximation. To derive the analytical expression for the optimal shape, we consider first the magnetic field generated above an idealized Hallbach magnet array of height h_m that extends to infinity in lateral directions. We assume the magnet to be mounted on a ferrro-magnetic plate reducing the problem to computing the magnetic field caused by the magnet strip $\{(x,y,z)\,|\,-\infty \leq x \leq \infty, -h_m \leq y \leq 0, -\infty \leq z \leq \infty\}$ in the overlying half-space $\{(x,y,z)\,|\,-\infty \leq x \leq \infty, 0 \leq y, -\infty \leq z \leq \infty\}$. We assumed the magnet to be magnetized in the y-direction in such a way that, given some amplitude M_0 and given some wavelength λ, the magnet's pre-magnetization vector $\mathbf{M}$ can be written as $\mathbf{M} = (0, M_0 \cos(\pi x/\lambda), 0)$. The problem is thus reduced to the coordinates x and y. Let μ_r denote the magnet's permeability. To solve the magnetic field problem in the air region, we solve the Laplace equation for scalar magnetic vector $\phi(x,y)$ supplied with appropriate boundary conditions. We proceed in a similar way to what for example [20] refers to as Type (a) magnet arrays and find that

$$\phi(x,y) = C_1 \cos(\pi\, x/\lambda) \exp(-\pi\, y/\lambda)\,, \tag{22}$$

where C_1 is an integration constant equal to

$$C_1 = \frac{M_0\, h_m}{\mu_r + \pi h_m/\lambda} \exp(\frac{\pi h_m}{\lambda})\,. \tag{23}$$

The magnetic field strength in the region above the magnet is therefore given by

$$\|\mathbf{B}\| = \mu_0 \sqrt{(\partial\phi/\partial x)^2 + (\partial\phi/\partial y)^2} = \mu_0 C_1 \pi/\lambda \exp(-\pi\, y/\lambda)\,, \tag{24}$$

and trivially satisfies Condition (2). In the derivation above, end-effect were neglected.

Hallbach arrays for magnetic density separation have been proposed in literature the [1]. To reduce the amount of magnetic material used however, a new design in which magnets magnetized in only upward direction and in which the magnet poles are interleaved with iron poles has been proposed in [4]. In this design the magnetic field distribution above the poles is brought into the desired shape by covering both the iron and magnetic poles with iron parts as shown in Figure 1. The air boundary of these ferromagnetic coverings are a line of constant the magnetic scalar potential. The optimal shape for this covering is thus know as soon as a scalar potential for the optimal field is known. This optimal scalar potential is given by (22) assuming no end-effects are

present. The optimal shape is thus found by setting $\phi(x, y)$ equal to a constant ϕ_0 and making the relationship between x and y explicit to obtain

$$C_{anal}(x) = \frac{\lambda}{\pi} \log[\cos(\frac{\pi\, x}{\lambda})] + C_2\,, \tag{25}$$

where $C_2 = \lambda/\pi(\log C_1 - \log \phi_0)$. For $\lambda = 0.06\,\mathrm{m}$ and $-\lambda/3 \leq x \leq \lambda/3$ this curve is shown as the curve Γ_b in Figure 3. This curve was used to shape the pole covers in Figure 1. In [4] is was verified numerically that a periodic continuation of the configuration shown in Figure 1 does give the a field distribution satisfying Condition (2).

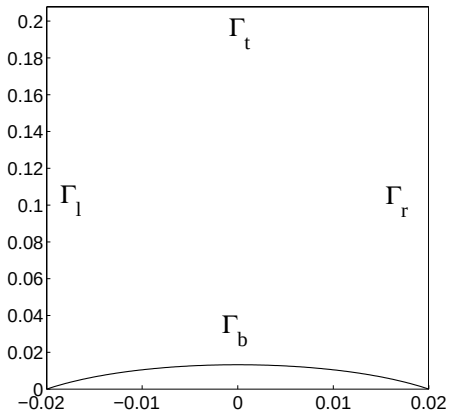

Figure 3: The computational domain Ω_p in the synthetic shape optimization problem.

The aim of the remainder of this subsection is to show that in a synthetic shape optimization algorithm that has the curve (25) as the optimal solution, our iso-geometric shape optimization algorithm converges to this optimum at the rate of convergence given by $\mathcal{O}(H^p)$, where H and p denote the meshwidth used to discretize the design curve and the polynomial degree of the spline approximation, respectively. This rate of convergence will be shown to be attained in the polynomial degree p is sufficiently high. To this end we define, given $\underline{y}(x)$ a smooth function in x and $\overline{y} = 0.2077\,\mathrm{m}$, the computational domain $\Omega_p = \{(x, y)\,|\, -\lambda/3 \leq x \leq \lambda/3,\, \underline{y}(x) \leq y \leq \overline{y}\}$ representing the air domain above a single magnetic pole. On this domain we consider solving the Laplace equation for the scalar potential ϕ subject to the exact solution (22) given on the boundary. The goal of the synthetic shape optimization algorithm is to minimize the functional

$$I_0[\phi; D] = \int_D \left(\frac{\partial \|\mathbf{B}\|^2}{\partial x} \right)^2 dx\, dy \tag{26}$$

where $D = [-0.02, 0.02] \times [0.06, 0.12]$ [m×m] by varying the shape of $\underline{y}(x)$. Motivating this choice for $I_0[\phi; D]$ is that if $\partial_x \|\mathbf{B}\| = 0$ then automatically $\partial_x(\partial_y \|\mathbf{B}\|) = \partial_y(\partial_x \|\mathbf{B}\|) = 0$ and Condition (2) is satisfied. The evaluation of this cost functional requires second order derivatives of the scalar potential ϕ. The curve $C_{anal}(x)$ is given by (25) is the analytical solution to this design problem. Let $C_{opt}(x)$ denote its approximation computed

numerically by the IGA shape optimization algorithm on the discretization defined by the following geometry knot vectors

$$\Xi_u = \{ \underbrace{0,\ldots,0}_{p+1 \text{ times}}, \tfrac{1}{32},\ldots,\tfrac{31}{32}, \underbrace{1,\ldots,1}_{p+1 \text{ times}} \} \quad \Xi_v = \{ \underbrace{0,\ldots,0}_{q+1 \text{ times}}, \tfrac{1}{5},\ldots,\tfrac{4}{5}, \underbrace{1,\ldots,1}_{q+1 \text{ times}} \}. \tag{27}$$

We compute the scaled L2-norm of the difference between $C_{opt}(x)$ and $C_{anal}(x)$ for $H \in \{\frac{1}{2}, \frac{1}{4}, \frac{1}{8}, \frac{1}{16}, \frac{1}{24}\}$, $p \in \{2,3,4\}$ and $q = p$. For $p = 3$, the afore mentioned choices of H leads to a problem with the number of design variables N_{dv} equal to $N_{dv} \in \{3,5,7,9,17,25\}$. Results are given in Figure 4.

Figure 4 (a) shows how the scaled error in the computed design curve decreased with the number of design variables N_{dv} for the three polynomial degrees. This figure shows that while for $p = 2$ the error only scales as $\mathcal{O}(H^{1/2})$, for $p = 3$ and $p = 4$ the error does scale according to $\mathcal{O}(H^p)$. The non-optimal convergence rate for $p = 2$ is likely to be due to the second order derivative of the second order approximation of ϕ causing a non-sufficiently smooth behaviour. For $p \geq 3$ however, the error scales with H as expected. Figure 4 (b) shows the error in the computed design curve as a function of x for the various values of H and for $p = 3$. This figures shows how the error is reduced as the spatial resolution is increased.

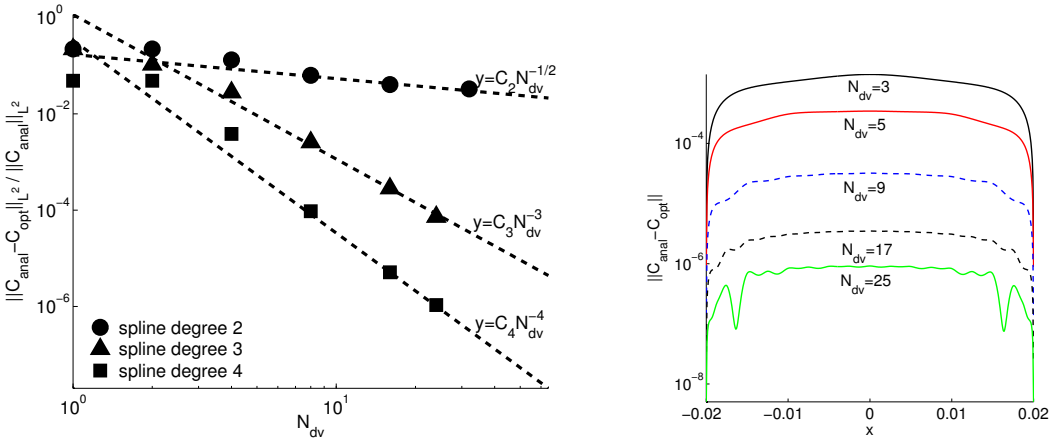

Figure 4: Verification of the isogeometric shape optimization algorithm: (a) convergence rate with respect to h-refinement for various spline degrees; (b) plot of the absolute error in the found shape for several levels of refinement, $p = q = 3$.

5.2. Shape Optimization of Pole Covers of Magnetic Density Separators

Before describing the application of the iso-geometric shape optimization algorithm to the density separator, we evaluate the cost functional (5) on the design proposed in [4] and shown in Figure 1. In all of the numerical experiments in this subsection we use the subdivision of the computational domain in patches shown in Figure 2 and a spline approximation of degree $p = 3 = q$. The cost function values obtained will serve as reference data in future comparisons. We evaluate the cost functional $I_0(A_z; D_1)$ and

$I_0(A_z; D_2)$, i.e., the dispersion $\partial\|\mathbf{B}\|/\partial y$ averaged over the domain D_1 and D_2 defined by (6) for both magnet-iron pole orderings given in Figure 1 and in Figure 5(a). The value for $\log_{10}[I_0(A_z; D_1)/\text{area}(D_1)]$ and $\log_{10}[I_0(A_z; D_2)/\text{area}(D_2)]$ for these two configurations are given in the first two lines of Table 1, respectively. The comparison of these two lines shows that assuring the end pole to be a magnet pole reduces the average dispersion in both D_1 and D_2. The numbers shown quantify the statement that switching the magnet-iron pole ordering around is effective in obtaining a more uniform field above the magnet array. To show the effect of the reduction of the dispersion on the distribution of $\|\mathbf{B}\|$ above the magnet array, we plotted in Figure 5(a) $\|\mathbf{B}\|(x, y)$ along three horizontal lines at height $y = 6\,\text{cm}$, $7\,\text{cm}$, and $8.5\,\text{cm}$. In Figure 5(b) we did the same for $\partial\|\mathbf{B}\|/\partial y$. By comparing Figure 5(a) with its equivalent in Figure 1(b), the improvement in field uniformity can clearly be seen. In the sequel of this section we will only consider configurations having a magnet as end pole. Figure 5(b) will act as a reference in the qualitative improvement of $\partial\|\mathbf{B}\|/\partial y$ by iso-geometric shape optimization.

The third and fourth lines of Table 1 demonstrate that the design of the magnet array can be further improved using iso-geometric shape optimization. These two lines list the average value of the dispersion $I_0(A_z; D_1)$ and $I_0(A_z; D_2)$ over the domain D_1 and D_2 for two geometries resulting from a the shape optimization process. The two optimization strategies differ in the choice of the objective domain. The third and fourth line of Table 1 correspond to choosing the objective domain Ω_0 defined (5) equal to $D_1 \cup D_2$ and D_1, respectively. These variants require 8 and 25 iterations to converge. The third line shows that the shape optimization process is successful in finding a geometry of the pole coverings that reduces the cost functional in both D_1 and D_2. The fourth line shows that excluding the exterior domain D_2 from the optimization allows to find a geometry with a lower cost functional in D_1 at the expense of a higher cost functional over D_2, demonstrating that the end-effects are harder to control than the interior domain.

In Figure 5(c)-(d) we plotted the geometry resulting from an optimization process with $D_1 \cup D_2$ as objective domain as well as the distribution of $\|\mathbf{B}\|$ and $\partial\|\mathbf{B}\|/\partial y$ over the magnet array. Compared with the initial geometry, the second pole (counting from the left) is lowered and the third pole covering is more asymmetric. The increased uniformity in both $\|\mathbf{B}\|$ and $\partial\|\mathbf{B}\|/\partial y$ can clearly be seen.

Figure 5(e)-(f) corresponds to D_1 as objective domain. Compared with the initial geometry, the second pole is lowered and the fourth pole is less rounded. Figure 5(f) shows that by excluding the exterior region from the design close to flat lines for $\partial\|\mathbf{B}\|/\partial y$ can be obtained. This is in stark contrast with the situation shown in Figure 5 (b) and shows that the optimization target set forth in Section can be reached in D_1.

Design	Ω_0	# it	$I_0(A_z; D_1)$	$I_0(A_z; D_2)$
magnet-pole ordering in [4]: Fig. 2	–	–	-3.072	-2.334
modified pole ordering: Fig. 5 (a) - (b)	–	–	-3.147	-2.55
IGA optimized: Fig. 5 (c) - (d)	$D_1 \cup D_2$	8	-3.926	-3.269
IGA optimized: Fig. 5 (e) - (f)	D_1	25	-4.755	-2.251

Table 1: Log_{10} of cost function value defined by (5) over the objective domains D_1 and D_2 for four designs of magnetic density separators.

Finally, let us return to the motivation of this work on reducing the end effects

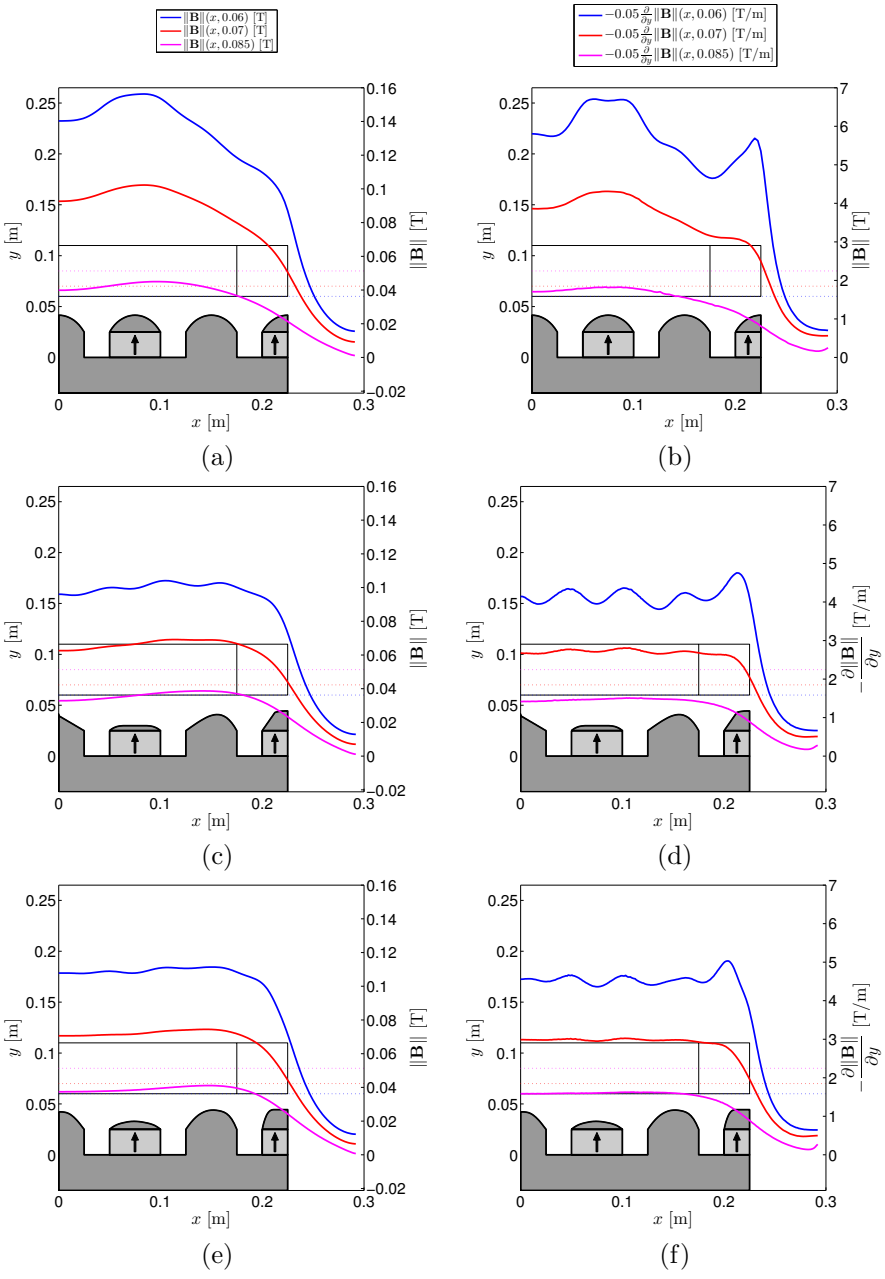

Figure 5: The graphs of $\|\mathbf{B}\|$ and $\frac{\partial\|\mathbf{B}\|}{\partial y}$ super imposed on the design. On the top (a), (b) the design from [4]. Below two optimized magnetic density separators that correspond to different objective domains Ω_0. (c),(d): $\Omega_0 = D_1 \cup D_2 = [0, 0.225] \times [0.06, 0.11]$. (e),(f): $\Omega_0 = D_1 = [0, 0.175] \times [0.06, 0.11]$.

left from D. Lahaye et al. [4]. Figure 5 show that our design reduces the end effects significantly, and thereby being promising for realistic industrial applications.

6. Conclusions

We developed an isogeometric analysis-based shape optimization algorithm and applied it to improvement of the design of a permanent magnet array for waste separation recently proposed in engineering literature. The distinct feature of our algorithm is the global nature of the update of the discretization at each step of the optimization algorithm. We verified the shape optimization algorithm in a synthetic problem with analytical solution and applied it to the realistic design problem. The design problem was solved up to the specifications resulting in new shapes for the ferromagnetic parts covering the poles in the array. This paper therefore contributes to the future developments of magnetic density separators.

Acknowledgment

Nguyen Dang Manh gratefully acknowledges the financial support from the European Community's Seventh Framework Programme FP7/2007-2013 under grant agreement number PITN-GA-2008-214584 (SAGA). Domenico Lahaye gratefully acknowledges Henk Polinder and Peter Rem for the many fruitful discussions during the course of this work.

References

[1] J. Svoboda. *Magnetic Techniques for the Treatment of Materials*. Kluwer, Dordrecht, The Netherlands, 2004.

[2] S. P. M. Berkhout E. J. Bakker and P. C. Rem. *Method and device for separating solid particles on the basis of a difference in density*. Patent EP 1800753/B1.

[3] Muchova L., E. J. Bakker, and P. Rem. Precious Metals in Municipal Solid Waste Incineration Bottom Ash. *Water Air Soil Pollution*, 9(1-2):107–116, 2009.

[4] D. Lahaye, H. Polinder, and P. Rem. Magnet designs for magnetic density separation of polymers. *The Journal of Solid Waste Technology and Management*, 26:977–983, 2011.

[5] T. Tadic and B.G. Fallone. Three-dimensional nonaxisymmetric pole piece shape optimization for biplanar permanent-magnet MRI systems. *Magnetics, IEEE Transactions on*, 47(1):231 –238, Jan. 2011.

[6] P. Di Barba and M.E. Mognaschi. Industrial design with multiple criteria: Shape optimization of a permanent-magnet generator. *Magnetics, IEEE Transactions on*, 45(3):1482 –1485, March 2009.

[7] D.H. Kim, J.K. Sykulski, and D.A. Lowther. The implications of the use of composite materials in electromagnetic device topology and shape optimization. *Magnetics, IEEE Transactions on*, 45(3):1154 –1157, March 2009.

[8] L. Saludjian, J.L. Coulomb, and A. Izabelle. Genetic algorithm and Taylor development of the finite element solution for shape optimization of electromagnetic devices. *Magnetics, IEEE Transactions on*, 34(5):2841 –2844, Sep 1998.

[9] Dong-Hun Kim, Se-Hee Lee, Il-Han Park, and Joon-Ho Lee. Derivation of a general sensitivity formula for shape optimization of 2-D magnetostatic systems by continuum approach. *Magnetics, IEEE Transactions on*, 38(2):1125 –1128, Mar 2002.

[10] T.J.R. Hughes, J.A. Cottrell, and Y. Bazilevs. Isogeometric analysis: CAD, finite elements, NURBS, exact geometry and mesh refinement. *Comput. Methods Appl. Mech. Engrg.*, 194(39-41):4135–4195, 2005.

[11] Yuri Bazilevs J.A. Cottrell, T.J.R. Hughes. *Isogeometric Analysis: Toward Integration of CAD and FEA*. J. Wiley., West Sussex, 2009.

[12] Seonho Cho and Seung-Hyun Ha. Isogeometric shape design optimization: exact geometry and enhanced sensitivity. *Struct. Multidiscip. Optim.*, 38(1):53–70, 2009.

[13] D. Manh Nguyen. *Isogemetric Analysis and Shape Optimization in Electromagnetics*. PhD thesis, Technical University of Denmark, 2012.

[14] D.M. Nguyen, A. Evgrafov, and J. Gravesen. Isogeometric shape optimization for electromagnetic scattering problems. *Progress in Electromagnetics Research B*, 46:117–146, 2012.
[15] R. E. Rosensweig. Magnetic fluids. *Ann. Rev.*, 19:437–463, 1987.
[16] P. P. Sylvester and R. L. Ferrari. *Finite Elements for Electrical Engineers*. Cambridge University Press, New York, third edition, 1996.
[17] Les Piegl and Wayne Tiller. *The NURBS book*. Springer-Verlag New York, Inc., New York, NY, USA, second edition, 1997.
[18] A. N. Pressley. *Elementary Differential Geometry*. Springer, second edition, 2010.
[19] P. Knupp and S. Steinberg. *Fundamentals of Grid Generation*. CRC Press, Boca Ranton, 1993.
[20] Han-Sam Cho, Chang-Hwan Im, and Hyun-Kyo Jung. Magnetic field analysis of 2-D permanent magnet array for planar motor. *Magnetics, IEEE Transactions on*, 37(5):3762 –3766, Sep 2001.